Giant monopole resonance strength in ^{40}Ca

D. H. Youngblood, Y.-W. Lui, and H. L. Clark
Cyclotron Institute, Texas A&M University, College Station, Texas 77842
(Received 2 December 1996)

The giant resonance region in ^{40}Ca was studied with inelastic scattering of 240 MeV α particles at small angles including 0°. A peak at $E_x = 17.5 \pm 0.4$ MeV with $\Gamma = 4.95 \pm 0.25$ MeV was found to contain $33 \pm 4\%$ of the isoscalar $E0$ energy-weighted-sum-rule (EWSR) strength and $57 \pm 6\%$ of the isoscalar $E2$ EWSR. Evidence was found for $92 \pm 15\%$ of the isoscalar $E0$ EWSR between $8 < E_x < 29$ MeV with a centroid of 18.9 ± 0.4 MeV and a rms half width of 11.1 MeV but a definitive $L = 0$ assignment could not be made. The resulting E_{GMR} is in agreement with systematics from heavier nuclei. [S0556-2813(97)03506-1]

PACS number(s): 24.30.Cz, 25.55.Ci, 27.40.+z, 27.80.+w

INTRODUCTION

The isoscalar giant monopole resonance (GMR) is of particular interest because its energy is directly related to the compressibility of nuclear matter (K_{nm}) [1]. In order to account for contributions from finite nuclei and extract K_{nm} macroscopic analyses [2] of the GMR require that the energy of the GMR be known in nuclei over a wide range of A. However, significant monopole strength has been located [2] in only a few nuclei with $A < 90$. In recent work [3] using inelastic scattering of 240 MeV α particles at 0° with a new spectrometer and beam analysis system, we obtained much better peak-to-background ratios for quadrupole and monopole resonances than previous works and were able to show that no more than 50% of the isoscalar $E0$ energy-weighted sum rule (EWSR) is present below $E_x = 25$ MeV in ^{58}Ni. In the scaling approximation, nuclear compressibility is related [1] to $E_{\mathrm{GMR}} = (m_3/m_1)^{1/2}$ where $m_k = \Sigma (E_n - E_0)^k |\langle 0|r^2|n\rangle|^2$, so this could have serious implications for nuclear compressibility.

The giant quadrupole (GQR) and monopole resonances in ^{40}Ca have been the subject of a number of theoretical investigations. Recently Kamerdzhiev *et al.* [4,5] have calculated both monopole and quadrupole strength distributions using a Hartree-Fock–RPA (random-phase approximation) including the continuum and ground-state correlations. There have been two studies of ^{40}Ca with inelastic scattering of α particles of $E_\alpha \approx 120$ MeV including scattering to 0° where monopole strength is enhanced. Brandenburg *et al.* [6] measured a limited range of excitation ($10 < E_x < 20$ MeV) and identified strength corresponding to 30% of the $E0$ EWSR. The work by Lui *et al.* [7] at $E_\alpha = 130$ MeV covered a wide range of excitation ($4 < E_x < 60$ MeV) but they were unable to definitively identify monopole strength. In this beam energy range, the (α, ^{5}Li) and (α, ^{5}He) reactions with subsequent decay of the mass five products into an α particle and a nucleon produce broad peaks in the α-particle spectrum corresponding to $24 < E_x < 46$ MeV in ^{40}Ca. These ''pickup-breakup'' peaks would obscure GMR strength above $E_x \approx 24$ MeV and may hamper determination of the continuum under the giant resonance peaks.

We have studied ^{40}Ca using 240 MeV α particles where the ''pickup-breakup'' peaks appear above $E_x = 40$ MeV, well outside of the region where GMR strength is expected. We report here results with excellent peak-to-background ratios at small scattering angles including 0°.

EXPERIMENTAL TECHNIQUE AND RESULTS

A beam of 240 MeV alpha particles from the Texas A&M K500 superconducting cyclotron bombarded a self-supporting natural Ca foil 11 mg/cm^2 thick located in the target chamber of the multipole-dipole-multipole spectrometer [8]. The beam was delivered to the spectrometer through a beam analysis system having two bends of 88° and 87° [9]. The beam was limited by slits after the first bend, and the second bend was used for clean up, with slits located so as not to intercept the primary beam. The horizontal acceptance of the spectrometer was 4° and ray tracing was used to reconstruct the scattering angle. The vertical acceptance was set at ±2°. When the spectrometer central angle (θ_{spec}) was set to 0°, the beam was stopped immediately in front of the detector in 5-cm-thick Ta. For $3.5° < \theta_{\mathrm{spec}} < 6°$, the beam was stopped beside the solid-angle defining slits. At larger angles the beam was stopped on a Faraday cup in the target chamber. At $\theta_{\mathrm{spec}} = 0°$, runs with an empty target frame had an α-particle rate about 1/2000 of that with a target in place. Alpha particles were present from the beam stop position tailing down in yield to about 5 MeV in equivalent excitation energy, then uniformly distributed over the rest of the spectrum.

The focal-plane detector [10] consisted of four proportional counters to measure x position at four points along a ray's path using the method of charge division, as well as an ionization chamber to provide ΔE and a scintillator to measure total energy and provide a fast timing signal for each ray. The out-of-plane scattering angle, ϕ, was not measured. To improve the quality of the position spectra, θ for each ray was calculated separately using data from independent wire pairs, and events in disagreement by more than two standard deviations were discarded [10]. Position resolution of approximately 0.9 mm and scattering angle resolution of about 0.09° were obtained. The angle calibration was obtained from an angle spectrum taken with a mask having five openings 0.01° wide spaced 1° apart. The actual spectrometer angle was determined from the kinematic cross-over from the elastic scattering off hydrogen (in the ^{12}C target) and

^{12}C inelastic-scattering peaks. The detector and calibration procedures are described in detail in Refs. [10, 11].

The position calibration of the focal plane required several steps. First, the centroids of peaks from elastic scattering from a thin ^{197}Au foil through the five-opening angle mask were obtained for ten dipole-field settings that spanned the useful length of the detector. These were compared with RAYTRACE [12] predictions to obtain the relationship between the channel number and position along the focal plane for each of the four position wires. Then data were taken with a ^{12}C target at the actual field settings used in the experiments. The positions of the first three excited states and four known [13] peaks up to $E_x = 23$ MeV in ^{12}C were used to obtain calibrations for each of the spectra.

The GOOSY (GSI online offline system) acquisition system [14] with a CAMAC crate hooked through a VME [15,16] interface to a DEC 4000-90 VAXSTATION was used for data acquisition. Typical data rates were 2500 events per sec with a live time of 75% while sorting all data to spectra for monitoring the experiment and writing all raw events to disk.

Giant-resonance data were taken with $\theta_{\rm spec}$ set at 0° and 3.5° covering the angular range from 0° to 5.5°. The excitation energy range observed was $2 < E_x < 30$ MeV.

Elastic- and inelastic-scattering data were taken at spectrometer angles of 3.5° and 5.9° at a different dipole field setting covering the range $-10 < E_x < 18$ MeV but with the spectrometer acceptance the same as for the giant resonance data. In addition, elastic- and inelastic-scattering data were taken over the angular range from 2° to 22° with the vertical acceptance of the spectrometer reduced to $\pm 0.8°$.

Each data set was divided into ten subsets, each corresponding to $\delta\theta = 0.4°$ using the angle obtained from ray tracing. ϕ is not measured by the detector, so the average angle for each bin was obtained by integrating over the height of the solid angle defining slit and the width of the angle bin. For comparison with theoretical calculations, the data points are plotted at this average angle so that, for example, data from the central angle bin taken with the spectrometer at 0° would be plotted at 1.08°. By plotting the data versus the average angle, the primary effect of the large solid angle is to fill in deep minima. The phase and cross-section maxima are affected only slightly. With the reduced vertical opening $[\pm 0.8°]$, the cross-section correction to the elastic scattering from averaging over the angle opening was 3% at 2.5° and less than 1% at larger angles except in the minima, when the averaged cross sections were plotted at the average angle determined as described above. This is particularly important for optical-model fits because the optical-model codes do not take into account averaging over a large vertical opening where the effective angular range for each data point is different.

Cross sections were obtained from the charge collected, target thickness, (measured by weighing) and known solid angle. The overall dead time of the electronics and computer data acquisition system was measured by passing pulses from a random (in time) pulser into the preamplifiers and through the entire system into the computer. They were checked by comparing the total number of pulses sent to the computer with the number in the spectra. Dead times obtained from the two methods agreed to within 1%. Approximately 33% of events which made it into the computer were discarded because the angles measured in the two sets of horizontal wires did not agree.

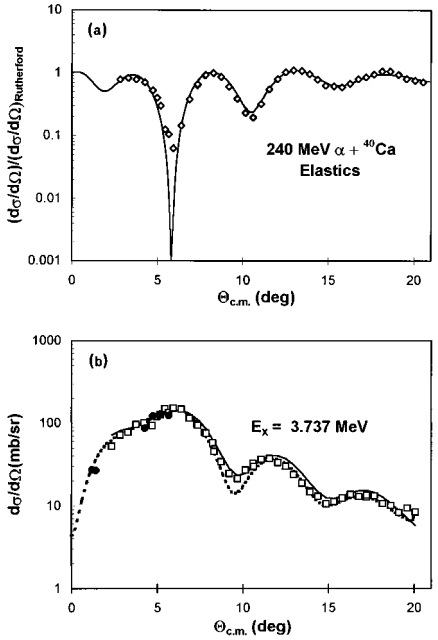

FIG. 1. (a) Angular distribution of the ratio of the differential cross section for elastic scattering to Rutherford scattering for 240 MeV α particles from Ca is plotted vs an average center-of-mass angle. The solid line shows an optical-model calculation using G194WS with the parameters from Table II. Statistical errors are smaller than the data points. (b) Angular distribution of the differential cross section for inelastic alpha scattering to the 3.737 MeV 3^- state in ^{40}Ca plotted vs an average center-of-mass angle. The open square data points were taken with the elastic data, while the solid round points are from the giant resonance data. The solid line shows an $L=3$ DWBA calculation using the deformed potential for $B(E3) = 0.0081\ e^2\ \mathrm{b}^6$. The dotted line shows a folding model calculation with $B(E3) = 0.0166\ e^2\ \mathrm{b}^6$. Statistical errors are smaller than the data points.

Angular distributions of the elastic scattering and inelastic scattering exciting the 3.737 MeV 3^- state are shown in Figs. 1(a) and 1(b), respectively. Data points obtained from both the giant-resonance and elastic-scattering runs are shown for the 3^- state, and are in good agreement. Giant-resonance spectra obtained at several angles are shown in Fig. 2. No background has been subtracted. Above $E_x = 12$ MeV the data were separated into several parts. The cross section for the giant-resonance peak was obtained by subtracting a ''background'' obtained by connecting the continuum above the peak with the yield below the peak in a smooth manner for each spectrum. The ''background'' is illustrated in Fig. 2 by the dotted line. The giant-resonance peak is centered at $E_x = 17.5 \pm 0.4$ MeV and has a rms half width of 4.95 MeV. The angular distribution of the cross section for this peak is shown in Fig. 3. Also shown are the angular distributions of the entire cross section for $12.9 < E_x < 29.9$ MeV. Attempts were then made to divide the peak into different components, both by fitting two broad Gaussian peaks simultaneously and narrow peaks to the fine structure at all angles and by slicing the peak into several

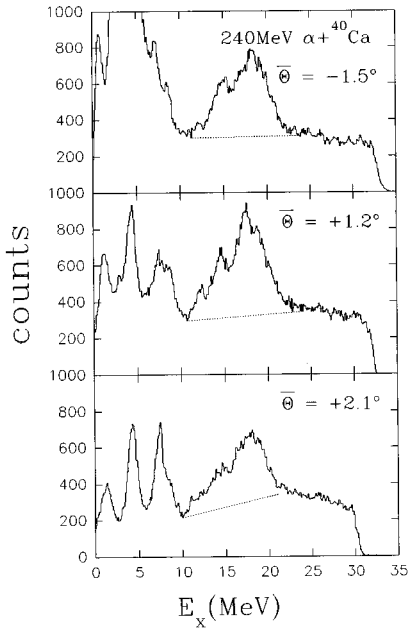

FIG. 2. Spectra obtained for Ca(α,α') at $E_\alpha=240$ MeV with $\theta_{\rm spec}=0°$ for three different angle gates. The top spectrum is from the left side of center, the middle spectrum near center, and the bottom spectrum from the right side of center. The angles shown are average angles obtained as described in the text. The dotted lines show the ''background'' assumed to get the peak yields.

distinct pieces. In each case, except for the known fine structure on the low-excitation side of the peak [6,7], the angular distributions for the different regions of the peak were very similar.

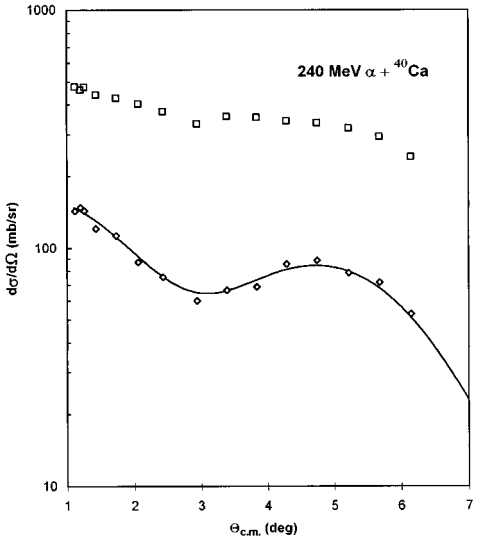

FIG. 3. Angular distribution of the differential cross section obtained for the giant-resonance peak (open diamonds) in ^{40}Ca is plotted vs an average center-of-mass angle. The open squares show the differential cross section for the entire region $12.9<E_x<29.9$ MeV. The solid line shows the DWBA calculation for 33% of the $E0$ EWSR plus 57% of the $E2$ EWSR plus 100% of the $E1$ EWSR for the GDR. Statistical errors are smaller than the data points.

DWBA AND OPTICAL-MODEL ANALYSIS

The transition densities and sum rules for various multipolarities are described thoroughly by Satchler [17]. The versions used for analyses in this work are given below.

The GMR has generally been considered a breathing mode oscillation and the corresponding transition density is given by [17]

$$U=-\alpha_0[3\rho+r d\rho/dr],$$

where, for a state that exhausts the EWSR [17],

$$\alpha_0^2=2\pi(\hbar^2/m)(A\langle r^2\rangle E_x)^{-1}.$$

For $L\geqslant 2$, the Bohr-Mottleson transition density was used,

$$U=-\beta R d\rho/dr,$$

and the EWSR is given by [17]

$$\sum (E_n-E_0)B_n(El)\uparrow = (\hbar^2/2m)[e^2Z^2l(2l+1)^2/A4\pi]\langle r^{2l-2}\rangle$$

and the deformation length $\beta_l R=\delta_l$ is determined from

$$B(El)\uparrow=|(l+2)\delta_l Z\langle r^{l-1}\rangle_p/4\pi|^2e^2.$$

The isovector $E1$ resonance in ^{40}Ca can be excited by the isoscalar α particle only through Coulomb excitation and for one state exhausting 100% of the sum rule [17]:

$$B(E1)\uparrow=(9\hbar^2NZe^2)/(4\pi 2mAE_x).$$

The isoscalar dipole resonance is described by Harakeh and Dieperink [18] as well as Giai and Sagawa [19] and the transition density is

$$U=-\beta[10\rho+3r^2\partial\rho/\partial r-5/3\langle r^2\rangle\partial\rho/\partial r + \epsilon(r\partial^2\rho/\partial r^2+4\partial\rho/\partial r)].$$

For 100% of the EWSR,

$$\beta^2=6\pi\hbar^2c^2/mAE_x[11\langle r^4\rangle-(25/3)\langle r^2\rangle^2-10\epsilon\langle r^2\rangle],$$

where $\epsilon=(4/E_2+5/E_0)(\hbar^2/3mA)$. E_2 is the energy of the GQR and E_0 is the energy of the GMR.

Inelastic alpha scattering to collective states has been analyzed [17] using either the deformed potential model or the folding model. Beene *et al.* [20] have shown that a consistent agreement between electromagnetic transition strengths and those measured with light- and heavy-ion inelastic scattering for low-lying 2^+ and 3^- states can only be obtained using the folding model. However, Beene *et al.* did not discuss excitation of the monopole resonance with alpha particles and there are no low-lying collective 0^+ states with which to test such calculations. Recently Satchler and Khoa [21], analyzing a 240 MeV α study of ^{58}Ni, compared results obtained using the deformed potential model, single folding using a Gaussian α-nucleon force with and without density dependence, and double folding using the BDM3Y1 nucleon-nucleon force which includes density dependence. Their conclusion was that each of the folding calculations

TABLE I. Deformation lengths for 100% of the respective sum rules in ^{40}Ca.

Isoscalar		E_x (MeV)
$L=0$	$\alpha_0 c=0.629$	18.0
$L=1$	$\beta_1 c=0.390$	20.0
$L=2$	$\beta_2 c=1.137$	17.7
$L=3$	$\beta_3 c=1.768$	18.0
$L=4$	$\beta_4 c=2.657$	18.0
Isovector		
$L=1$	$B(E1)=0.07424e^2$ b	19.0

gave very similar 0° cross sections for the GMR, and fit the data for the 4.475 MeV 3^- state using the electromagnetic $B(E3)$ value. Deformed potential calculations required a $B(E3)$ value about a factor of 2 below the electromagnetic value to fit the experimental data for the 4.475 MeV state. However, if the potential deformation length was set equal to the mass deformation length ($\alpha_m c=\alpha_p R_p$) for the GMR, then nearly the same 0° cross section was obtained with the deformed potential as with the folding models. They also concluded that the larger-angle elastic-scattering data could not be fit using the folded potential shapes for both the real and imaginary terms of the potential. Thus, they did a hybrid calculation where the real parts of the optical potential and the form factor were obtained by folding, but the imaginary potential was Woods-Saxon and the imaginary part of the form factor was obtained using the deformed potential model.

Since Satchler and Khoa showed that each of the folding models gave similar results both for the giant-resonance and low-lying states, we have chosen to use the simpler single folding without density dependence but with a Woods-Saxon imaginary term. For this we use the same Gaussian α-nucleon interaction with range 1.94 fm used by Satchler [17] and Satchler and Khoa [21] where the amplitude of the interaction is varied to fit the elastic scattering. This calculation is referred to as G194WS. A Fermi mass distribution with $c=3.65$ fm and $a=0.55$ fm assuming identical neutron and proton distributions was used for ^{40}Ca. We also show results obtained with a deformed potential model.

Distorted-wave Born approximation (DWBA) and optical-model calculations were carried out with the code PTOLEMY [22]. Input parameters for PTOLEMY were modified [23] to obtain a relativistic kinematically correct calculation. Folded potentials and form factors were obtained using the code DOLFIN [24] based on the work by Satchler and Love [25]. The amplitudes of the transition densities for the various multipoles obtained from the expressions above for 100% of the respective sum rules are given in Table I.

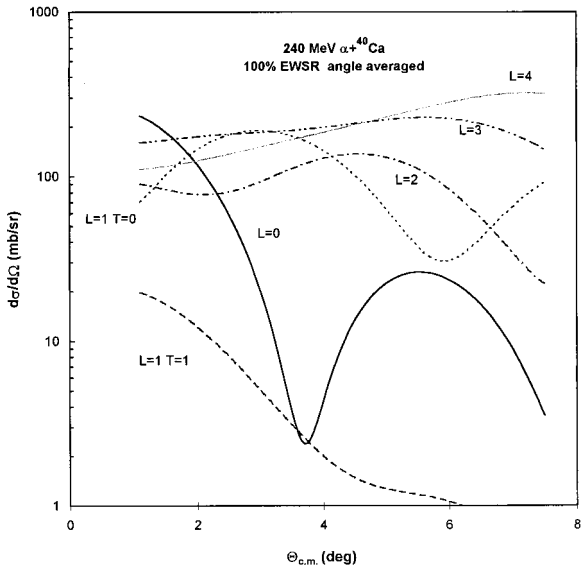

FIG. 4. Angular distributions of the differential cross sections for various multipoles calculated with G194WS for 100% of the respective sum rules using deformation lengths from Table I.

Optical-model parameters and the amplitude of the real part of the α-nucleon interaction were obtained for ^{40}Ca by fitting the elastic scattering, and the resulting fits are shown in Fig. 1(a). The parameters are listed in Table II. DWBA calculations using the deformed potential model and G194WS were carried out for the $E_x=3.737$ MeV 3^- state and are shown superimposed on the data in Fig. 1(b). The $B(E3)$ value obtained with the deformed potential is about a factor of 2 lower than the electromagnetic value, but in agreement with other α-scattering measurements analyzed with the deformed potential model while the G194WS fits the data well with a $B(E3)$ value about 4% smaller than the electromagnetic value. The absolute cross section was checked by comparing optical-model calculations to small-angle elastic scattering which is dominated by Rutherford scattering. From this we estimate that the uncertainty in the absolute cross section is about $\pm 5\%$. The cumulative uncertainties in target thickness, solid angle, etc., would result in about a $\pm 10\%$ uncertainty.

Angular distributions for the different multipoles that might contribute between $E_x=10$ and 30 MeV calculated with G194WS are shown in Fig. 4 for 100% of the respective EWSR. The striking characteristic of monopole strength is the strong peaking at 0° of the cross section where the monopole would be by far the largest contribution. Thus, the GMR strength would be characterized by strong forward peaking in the angular distribution. The isovector giant-dipole resonance (GDR) is also forward peaked (excited only by Coulomb excitation in ^{40}Ca), but is much weaker than the other multipolarities.

TABLE II. Optical-model parameters obtained from fits to elastic scattering.

	V (MeV)	R (fm)	a (fm)	W (MeV)	R_i (fm)	a_i (fm)	R_c (fm)
G194WS	24.7	-	-	23.8	4.852	0.755	4.446
Woods-Saxon	61.0	4.860	0.580	23.6	4.726	0.971	4.446

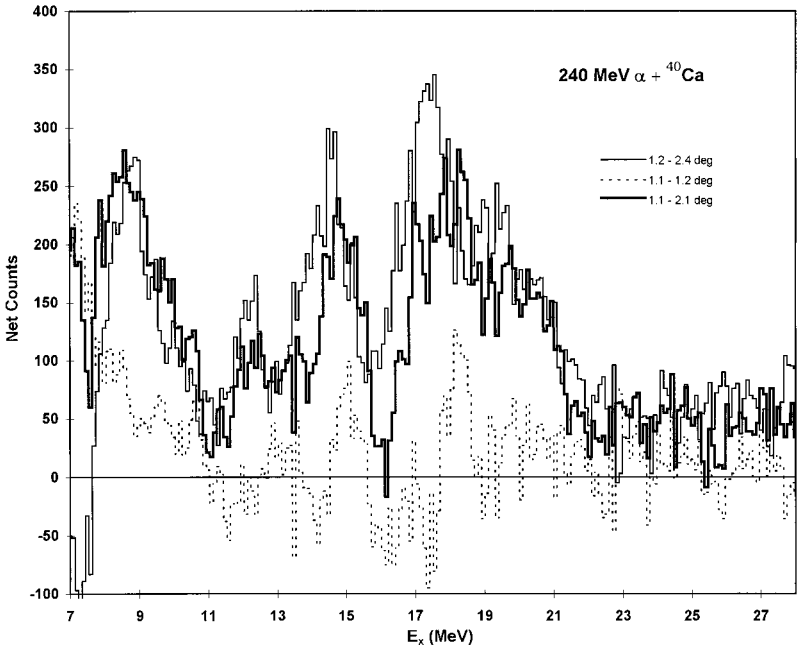

FIG. 5. Difference spectra obtained as described in the text. The thin solid line results from subtracting the spectrum for $\theta=2.4°$ from the spectrum for $\theta=1.2°$. The dashed line is for 1.1°–1.2° and the thick line for 1.1°–2.1°.

In deformed-potential calculations for the monopole resonance, generally it has been customary to adopt the uniform mass model and set $R^2=(5/3)\langle r^2\rangle$ and then use the potential radius (R_p) for R. Since $R_p^2\simeq(5/3)\langle r^2\rangle_m$ in heavier nuclei, this has the effect of setting the mass deformation parameter equal to the potential deformation parameter ($\alpha_m=\alpha_p$). However, Satchler [17] has pointed out that, to be consistent with what is done for other multipolarities, the deformation lengths should be equal ($\alpha_m c=\alpha_p R_p$), which has the effect of lowering the cross sections obtained with the deformed potential model by the factor $(c/R_p)^2$. The 0° cross section obtained for the GMR in ^{40}Ca was 329 mb/sr with G194WS 336 mb/sr with the deformed potential assuming $\alpha_m c=\alpha_p R_p$, and 561 mb/sr with the deformed potential assuming $R_p^2=(5/3)\langle r^2\rangle$.

DISCUSSION

Fits to the angular distribution of the giant resonance peak were carried out with a sum of isoscalar 0^+, 2^+ and isovector 1^- strengths. The GDR is located at about $E_x=19$ MeV in ^{40}Ca [26]. The strength of the isovector giant-dipole resonance was fixed at 100%, and the others were allowed to vary to minimize χ^2. An excellent fit was obtained with 33 ± 4% of the $E0$ EWSR and 57 ± 6% of the $E2$ EWSR. The result is shown by the solid line in Fig. 3. An excellent fit was obtained with about the same χ^2 with 42% of the $E0$ EWSR and 57% of the $E2$ EWSR if no isovector 1^- strength was included. The $E2$ strength observed is in agreement with other works [7].

We attempted to estimate the total $E0$ strength in the continuum between $12.9<E_x<29.9$ MeV using the same procedures described in our recent work investigating ^{58}Ni [3] where we were able to set an upper limit on the amount of $E0$ strength in the continuum. The angular distribution of the continuum cross section was fit with a sum of isoscalar 0^+, 2^+, 1^-, 3^-, and 4^+ and a linear (with θ) background. For ^{40}Ca however, we found that excellent fits could be obtained with $E0$ strength ranging from 15 to 75 % of the EWSR depending on strengths of the other multipolarities. Hence, with 32% of the $E0$ EWSR in the peak, up to 100% of the $E0$ EWSR might be present below $E_x=27$ MeV, in sharp contrast to ^{58}Ni where a similar analysis showed that less than half of the $E0$ EWSR could be present in the same region. A comparison of the angular distributions of the continuum for the two nuclei shows that in ^{58}Ni, the cross section was essentially flat below 4°, whereas in Ca the cross section continues to rise and peaks at the smallest angle, indicating the presence of monopole strength. In Ca it was not possible to draw conclusions about the strength of the higher multipoles in the continuum, as differing combinations of $L>2$ multipoles and background assumptions could fit the data equally well. However, approximately 40% of the $E2$ EWSR was required for all the fits to the angular distribution of the continuum, suggesting that the $E2$ strength not seen in the peak is present in the continuum below $E_x=27$ MeV.

Since the $E0$ angular distribution is strongly peaked near 0°, and the angular distributions for the other multipolarities are nearly flat below 2°, a spectrum of $E0$ strength can be obtained from the data taken with the spectrometer at 0° by subtracting spectra obtained from an angle cut corresponding to angles near the edges of the slit ($\theta=2°$) from spectra taken near the center ($\theta=0°$) [6]. In Fig. 5 subtracted spectra are shown for two different sets of angle pairs. They are very similar, and the result from a smaller angle difference also has a lower yield as expected. Also shown is the difference between two spectra in adjacent nearly central angle bins and the result is very nearly 0 over the entire range from $E_x=8$ to 28 MeV. The resulting ''difference'' spectra were converted to cross section and then adjusted to a 0° cross section using the DWBA predictions for the GMR, correcting the overall cross section for the known GQR and GDR contributions. The resulting cross section for $E0$ excitation is shown in Fig. 6. The excitation energy dependence of the 0° GMR cross section for 100% of the EWSR was calculated

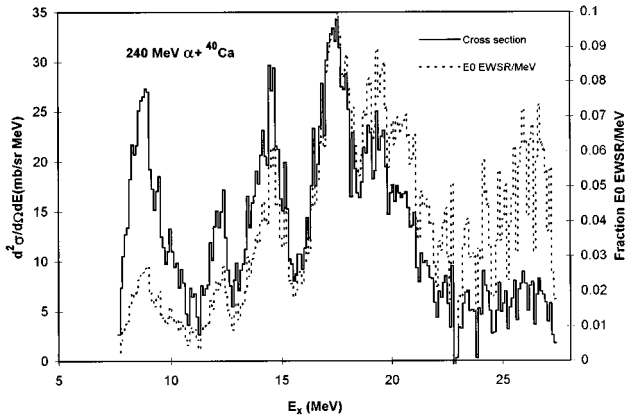

FIG. 6. The solid line shows the double-differential cross section for 0° $E0$ strength obtained from the difference between spectra taken at $\theta=1.1°$ and at $\theta=2.4°$ obtained as described in the text. The dashed line shows a spectrum of the fraction of the $E0$ EWSR obtained from the same difference spectrum.

with DWBA and is shown in Fig. 7. The cross section falls rapidly with increasing excitation energy, so strong cross sections at low excitation may not contribute as much to the sum rule as weak cross sections at high excitation. A ''spectrum'' of the ''fraction of the $E0$ EWSR'' as a function of E_x was calculated by dividing the cross section shown in Fig. 6 by the DWBA prediction. This is also shown in Fig. 6. Here it can be seen that the relatively strong peak at $E_x=8$ MeV makes only a small contribution to the sum-rule strength and that the small cross section above $E_x=22$ MeV contributes significantly to the sum-rule strength. In addition to the $\pm5\%$ uncertainty in the absolute cross section, a source of uncertainty that is of particular importance for the subtracted spectra is the relative solid angles for each of the spectra determined from software cuts on θ. From the angle calibrations, we estimate that the relative solid angles are uncertain by $\pm2.5\%$ between the 1.1° spectrum and the 2.4° spectrum. This results in a $\pm15\%$ uncertainty in the cross sections obtained from the difference spectra.

Brandenburg *et al.* [6] also obtained an $E0$ strength distribution in ^{40}Ca from inelastic alpha scattering by subtract-

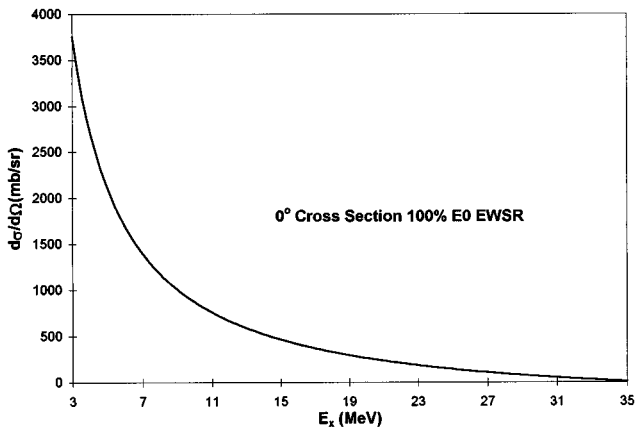

FIG. 7. The solid line shows the 0° $E0$ cross section for 100% of the $E0$ EWSR as a function of excitation energy calculated with G194WS.

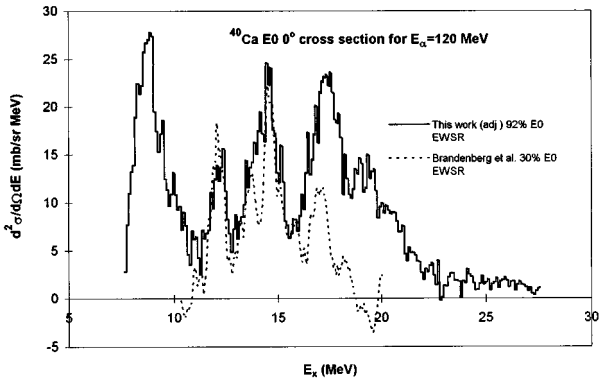

FIG. 8. The 0° cross section for $E0$ strength at $E_\alpha=120$ MeV obtained from our data is shown by the solid line. The dashed line shows the $E0$ strength seen by Brandenburg *et al.* [6] corrected to a 0° cross section as described in the text.

ing spectra taken at two angles. In order to compare our results with theirs, we performed DWBA calculations for $E_\alpha=120$ MeV using optical parameters from Ref. [27], and converted our data to an expected 0° cross sections at $E_\alpha=120$ MeV. We also corrected their cross sections to 0° cross sections and smeared their data to approximate our resolution. Their data are compared to our adjusted data in Fig. 8. Their data were limited to $10<E_x<20$ MeV and it can be seen that there is excellent agreement with peak positions and amplitudes at lower excitation, but the peaks in their data become progressively weaker at higher excitation, and the net cross section becomes negative near $E_x=20$ MeV, suggesting that in this region over subtraction occurred, possibly from some continuum excitation and/or other background that was energy and angle dependent. As their data did not extend beyond $E_x=20$ MeV, such a background, if it existed, could not be seen. The similarity of the $E0$ structure seen in the two experiments with very different experimental conditions and different bombarding energies increases confidence that this structure is due to $E0$ strength in ^{40}Ca and not an artifact of the reaction or experiment.

The sum-rule strengths (m_1) obtained for three excitation regions are listed in Table III. The centroid energies, as well as $(m_1/m_{-1})^{1/2}$, $(m_2/m_0)^{1/2}$, and $(m_3/m_1)^{1/2}$ obtained from the two difference spectra are given in Table IV. The errors shown are statistical only. The total strength seen in the two spectra ($92\pm2\%$ and $96\pm3\%$ of the $E0$ EWSR) agrees within statistical errors. With the $\pm15\%$ uncertainty in absolute cross section for the subtracted spectra, the total $E0$ strength is consistent with 100% of the $E0$ EWSR without

TABLE III. Monopole-resonance sum-rule strengths for ^{40}Ca obtained from difference spectra. Errors are statistical only.

	Spectrum	
E_x range (MeV)	1.1°–2.4° %$E0$ EWSR	1.1°–2.1° %$E0$ EWSR
7.5–12.5	7.6±0.2	10.8±0.3
12.5–22.5	50.0±1.4	51.6±1.3
22.5–28.8	34.7±1.7	33.1±2.3
7.5–28.8	92 ±2	96 ±3

TABLE IV. Monopole-resonance parameters for ^{40}Ca obtained from difference spectra. Errors are statistical only.

	Spectrum	
	1.1°–2.4°	1.1°–2.1°
E_{avg} (MeV)	18.89±0.11	18.17±0.15
$(m_1/m_{-1})^{1/2}$ (MeV)	17.29±0.12	17.03±0.13
$(m_2/m_0)^{1/2}$ (MeV)	4.70±0.11	4.65±0.21
$(m_3/m_1)^{1/2}$ (MeV)	21.30±0.12	20.85±0.16

considering other sources of uncertainty (DWBA method, deficiencies in the spectrum subtraction technique for identifying $E0$ strength, etc.). Except for the region $7.0<E_x<12.5$ MeV, the $E0$ strengths in the two spectra agree within statistics. The values obtained for the centroids and $(m_3/m_1)^{1/2}$ obtained from the two spectra disagree by more than the statistical uncertainty because the 1.1°–2.1° data show somewhat more strength between 7.5 and 9 MeV than the 1.1°–2.4° data. This is due to a ''tail'' of alpha particles extending from the low excitation edge of the detector to about $E_x=8.5$ MeV, probably from secondary scattering of elastics from low excitation edge of the detector entrance window. This ''tail'' showed only in the spectra on one side of 0°, consistent with this source. Thus the results from the 1.1°–2.4° data that do not have this tail are probably the most reliable.

The value of $(m_3/m_1)^{1/2}*A^{1/3}$ obtained, 72.1±0.4 MeV, follows excellently the trend for heavier nuclei as can be seen in Fig. 9(a) where the results for all nuclei where 100% of the $E0$ EWSR has been identified are shown. Recently Blaizot *et al.* [28] have calculated monopole energies $E_0=(m_1/m_{-1})^{1/2}$ with a Gogny effective interaction which yields $K_{nm}=209$ MeV. The rms Coulomb radius for ^{40}Ca calculated with this interaction is 3.470 fm, close to the value

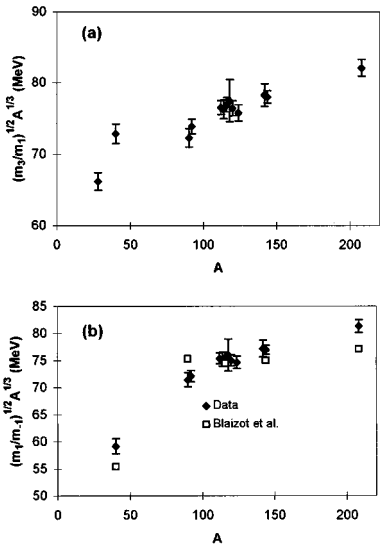

FIG. 9. (a) $E_{GMR}*A^{1/3}$ is shown as a function of A for nuclei where reported experimental data is consistent with 100% of the $E0$ EWSR [2]. (b) $(m_1/m_{-1})^{1/2}*A^{1/3}$ obtained by Blaizot *et al.* [28] is plotted for several nuclei along with the centroid energies of the GMR obtained for nuclei $A\geq 90$ and $(m_1/m_{-1})^{1/2}*A^{1/3}$ we obtain for ^{40}Ca.

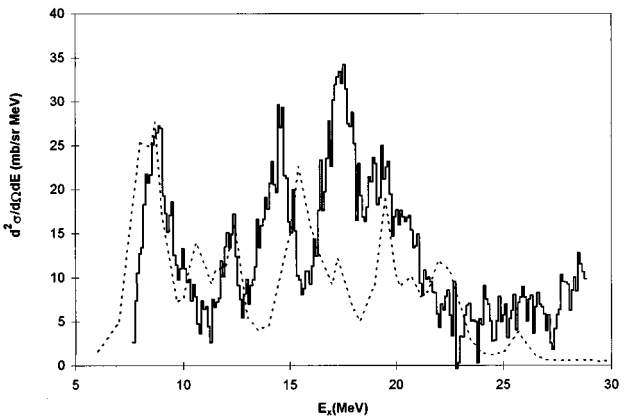

FIG. 10. The 0° cross section for $E0$ strength in ^{40}Ca(α, α'), obtained as described in the text, is shown by the solid line. The dashed line shows a ^{40}Ca(α, α') 0° cross section calculated from the isoscalar $E0$ strength function of Ref. [5].

3.488 fm obtained with the mass distribution parameters used in our work. In this calculation they included contributions from pairing which become more important in lighter nuclei. They obtain $(m_1/m_{-1})^{1/2}=16.2$ MeV for ^{40}Ca, in reasonable agreement with the value we obtain of 17.3 ±0.4 MeV. Figure 9(b) shows the values of $(m_1/m_{-1})^{1/2}*A^{1/3}$ obtained by Blaizot for 5 nuclei, compared to the centroid energies of the GMR (times $A^{1/3}$) for all nuclei with $A>89$ where 100% of the $E0$ EWSR has been identified. The general trend of the data is reproduced, though the experimental values clearly increase more rapidly between $A=90$ and 208 than do the calculated values.

Kamerdzhiev *et al.* [4,5] carried out a continuum RPA calculation of $E0$ strength in ^{40}Ca including 1p1h, 2p2h and ground-state correlations. The expected 0° inelastic alpha scattering cross section for isoscalar $E0$ strength in ^{40}Ca obtained from the strength distribution calculated by Kamerdzhiev *et al.* [5] is shown in Fig. 10 along with our 0° $E0$ cross section. The 8 and 12 MeV experimental peaks are predicted well both in position and strength, however at higher excitation energy there is a poor correlation and the experimental strength considerably exceeds the strength predicted in the calculation which corresponds to $4250\,e^2$ fm^4 MeV, or 52% of the isoscalar $E0$ EWSR. In a footnote, Kamerdzhiev *et al.* [5] state that the remaining strength is ''between $E_x=30$ and 80 MeV.'' They show slightly less strength below $E_x=30$ MeV with a straight 1p1h+continuum calculation. This is in sharp contrast to a calculation by Van Giai and Sagawa [19] with 1p1h+continuum where nearly 100% of the isoscalar $E0$ sum rule is predicted to lie below $E_x=30$ MeV in ^{40}Ca. Our data would suggest that though Kamerdzhiev *et al.* predict some of the fine structure nicely, their calculation pushes about half the $E0$ strength up to too high an energy.

In an earlier work [3] on ^{58}Ni, we established an upper limit of 50% of the $E0$ EWSR in the region $E_x<25$ MeV by fitting the angular distributions of the cross sections. The same spectrum subtraction technique that was used in this work to (tentatively) identify essentially all of the $E0$ strength in ^{40}Ca was also applied to the ^{58}Ni data. Using the subtracted spectra for ^{58}Ni, we obtained an $E0$ distribution in the same manner as for ^{40}Ca. The $E0$ strength obtained is

consistent with that reported in Ref. [3]. Using the DWBA calculations from Ref. [3] (deformed potential and uniform mass model) about 35% of the $E0$ EWSR is seen in two peaks at about $E_x = 17$ and 20 MeV and little $E0$ strength is seen in the continuum above the peaks.

Thus the conclusion is somewhat different from Ref. [3]. Only about 50% of the $E0$ EWSR is accounted for in ^{58}Ni [3,21], but there is evidence for strength exhausting nearly 100% of the $E0$ EWSR in ^{40}Ca below $E_x = 29$ MeV. The model dependence of the $E0$ EWSR strength remains a problem [21,29]. In heavier nuclei such as ^{116}Sn [21] and ^{208}Pb [29] use of the folding model or the deformed potential model with $\alpha_m c = \alpha_p R_p$ result in $E0$ EWSR values considerably exceeding 100%. If this is also true in light nuclei, more $E0$ strength may lie at higher excitation in ^{40}Ca. This is consistent with the experimental $E0$ EWSR distribution shown in Fig. 6 which continues high at the highest excitation energy measured.

This work was supported in part by the Department of Energy under Grant No. DE-FG03-93ER40773 and by the Robert A. Welch Foundation.

[1] J. P. Blaizot, Phys. Rep. **64**, 171 (1980).
[2] S. Shlomo and D. H. Youngblood, Phys. Rev. C **47**, 529 (1993).
[3] D. H. Youngblood, H. L. Clark, and Y.-W. Lui, Phys. Rev. Lett. **76**, 1429 (1996).
[4] S. Kamerdzhiev, J. Speth, and G. Tertychny, Phys. Rev. Lett. **74**, 3943 (1995).
[5] S. Kamerdzhiev, G. Tertychny, J. Speth, and J. Wambach, Nucl. Phys. **A577**, 641 (1994).
[6] S. Brandenburg, R. De Leo, A. G. Drentje, M. N. Harakeh, H. Sakai, and A. van der Woude, Phys. Lett. **130B**, 9 (1983).
[7] Y.-W. Lui, J. D. Bronson, C. M. Rozsa, D. H. Youngblood, P. Bogucki, and U. Garg, Phys. Rev. C **24**, 884 (1981).
[8] D. M. Pringle, W. N. Catford, J. S. Winfield, D. G. Lewis, N. A. Jelley, K. W. Allen, and J. H. Coupland, Nucl. Instrum. Methods Phys. Res. A **245**, 230 (1986).
[9] D. H. Youngblood and J. D. Bronson, Nucl. Instrum. Methods Phys. Res. A **361**, 37 (1995).
[10] D. H. Youngblood, Y.-W. Lui, H. L. Clark, P. Oliver, and G. Simler, Nucl. Instrum. Methods Phys. Res. A **361**, 539 (1995).
[11] H. L. Clark, Y.-W. Lui, and D. H. Youngblood, Nucl. Phys. **A589**, 416 (1995).
[12] S. Kowalski and H. A. Enge, unpublished.
[13] F. Ajzenberg-Selove, Nucl. Phys. **A506**, 1 (1990).
[14] Received from H. G. Essel, GSI, Gesellschaft für Schwerionenforschung, Darmstadt, Germany.
[15] H. Dejbakhsh and K. Hagel, Texas A&M University report, 1994 (unpublished), p. 134.
[16] D. Yoder, private communication.
[17] G. R. Satchler, Nucl. Phys. **A472**, 215 (1987).
[18] M. N. Harakeh and A. E. L. Dieperink, Phys. Rev. C **23**, 2329 (1981).
[19] Nguyen Van Giai and H. Sawaga, Nucl. Phys. **A371**, 1 (1981).
[20] J. R. Beene, D. J. Horen, and G. R. Satchler, Phys. Lett. B **344**, 67 (1995).
[21] G. R. Satchler and Dao T. Khoa, Phys. Rev. C **55**, 285 (1997).
[22] M. Rhoades-Brown, M. H. Macfarlane, and S. C. Pieper, Phys. Rev. C **21**, 2417 (1980); M. H. Macfarlane, and S. C. Pieper, Argonne National Laboratory Report No. ANL-76-11, Rev. 1, 1978, unpublished.
[23] G. R. Satchler, Nucl. Phys. **A540**, 533 (1992).
[24] L. D. Rickertsen, The folding program DOLFIN, 1976, unpublished.
[25] G. R. Satchler and W. G. Love, Phys. Rep. **55**, 183 (1979).
[26] A. Veyssiére, H. Beil, R. Bergeére, P. Carlos, A. Leprêtre, and A. de Miniac, Nucl. Phys. **A227**, 513 (1974).
[27] D. H. Youngblood, J. M. Moss, C. M. Rozsa, J. D. Bronson, A. D. Bacher, and D. R. Brown, Phys. Rev. C **13**, 994 (1976).
[28] J. P. Blaizot, J. F. Berger, J. Decharge, and M. Girod, Nucl. Phys. **A591**, 435 (1995).
[29] D. H. Youngblood, Phys. Rev. C **55**, 950 (1997).